Icarus 206 (2010) 485–497

Contents lists available at ScienceDirect

Icarus

journal homepage: www.elsevier.com/locate/icarus

Impact cratering records of the mid-sized, icy saturnian satellites

Michelle R. Kirchoff *, Paul Schenk

Lunar and Planetary Institute, 3600 Bay Area Blvd., Houston, TX 77058, United States

ARTICLE INFO

Article history:
Received 20 December 2008
Revised 30 November 2009
Accepted 3 December 2009
Available online 14 December 2009

Keywords:
Saturn
Satellites, surfaces
Cratering

ABSTRACT

Resolution of *Voyager* 1 and 2 images of the mid-sized, icy saturnian satellites was generally not much better than 1 km per line pair, except for a few, isolated higher resolution images. Therefore, analyses of impact crater distributions were generally limited to diameters (D) of tens of kilometers. Even with the limitation, however, these analyses demonstrated that studying impact crater distributions could expand understanding of the geology of the saturnian satellites and impact cratering in the outer Solar System. Thus to gain further insight into Saturn's mid-sized satellites and impact cratering in the outer Solar System, we have compiled cratering records of these satellites using higher resolution *Cassini ISS* images. Images from *Cassini* of the satellites range in resolution from tens m/pixel to hundreds m/pixel. These high-resolution images provide a look at the impact cratering records of these satellites never seen before, expanding the observable craters down to diameters of hundreds of meters. The diameters and locations of all observable craters are recorded for regions of Mimas, Tethys, Dione, Rhea, Iapetus, and Phoebe. These impact crater data are then analyzed and compared using cumulative, differential and relative (R) size-frequency distributions. Results indicate that the heavily cratered terrains on Rhea and Iapetus have similar distributions implying one common impactor population bombarded these two satellites. The distributions for Mimas and Dione, however, are different from Rhea and Iapetus, but are similar to one another, possibly implying another impactor population common to those two satellites. The difference between these two populations is a relative increase of craters with diameters between 10 and 30 km and a relative deficiency of craters with diameters between 30 and 80 km for Mimas and Dione compared with Rhea and Iapetus. This may support the result from *Voyager* images of two distinct impactor populations. One population was suggested to have a greater number of large impactors, most likely heliocentric comets (Saturn Population I in the *Voyager* literature), and the other a relative deficiency of large impactors and a greater number of small impactors, most likely planetocentric debris (Saturn Population II). Meanwhile, Tethys' impact crater size-frequency distribution, which has some similarity to the distributions of Mimas, Dione, Rhea, and Iapetus, may be transitional between the two populations. Furthermore, when the impact crater distributions from these older cratered terrains are compared to younger ones like Dione's smooth plains, the distributions have some similarities and differences. Therefore, it is uncertain whether the size-frequency distribution of the impactor population(s) changed over time. Finally, we find that Phoebe has a unique impact crater distribution. Phoebe appears to be lacking craters in a narrow diameter range around 1 km. The explanation for this confined "dip" at $D = 1$ km is not yet clear, but may have something to do with the interaction of Saturn's irregular satellites or the capture of Phoebe.

1. Introduction

Images from *Voyager* 1 and 2 provided an amazing first up-close look of the saturnian satellites, which allowed researchers to explore many features of these satellites (e.g., Shoemaker and Wolfe, 1981; Smith et al., 1981, 1982; Strom and Woronow, 1982; Chapman, 1983; Hartmann, 1984; Horedt and Neukum, 1984; Morrison et al., 1984, 1986; Plescia and Boyce, 1985; Squyres and Croft, 1986; Squyres et al., 1987; Lissauer et al., 1988; Kargel and Pozio, 1996). *Voyager* images, however, were generally not much better than approximately 1 km per line pair with some exceptions that achieved several hundred meters per line pair for small regions (Smith et al., 1981, 1982; Plescia and Boyce, 1985; Morrison et al., 1986; Lissauer et al., 1988). Because the ability to recognize impact craters is dependant on the image resolution (the crater diameter generally has to be $\sim 5\times$ the image resolution), analysis of impact crater distributions was limited to diameters (D) of a few to tens of kilometers with *Voyager* images. With this data some important issues were raised, but unable to be satisfactorily resolved.

* Corresponding author. Present address: Southwest Research Institute, 1050 Walnut Street, Suite 300, Boulder, CO 80302, United States. Fax: +1 281 486 2162.
E-mail addresses: kirchoff@boulder.swri.edu (M.R. Kirchoff), schenk@lpi.usra.edu (P. Schenk).

0019-1035/$ - see front matter © 2009 Elsevier Inc. All rights reserved.
doi:10.1016/j.icarus.2009.12.007

One of these issues was the number of distinct impactor populations in the saturnian system and their origins. To many (Shoemaker and Wolfe, 1981; Smith et al., 1981, 1982; Strom and Woronow, 1982; Horedt and Neukum, 1984; Plescia and Boyce, 1985; Chapman and McKinnon, 1986; Strom, 1987b; Kargel and Pozio, 1996) the cratering data seemed to imply that two different impactor populations were recorded. One population was characterized by a greater number of larger craters (Saturn Population I in *Voyager* literature), while a greater number of smaller craters characterized the second population (Saturn Population II). Furthermore, Population I was found on older terrains, including Rhea and Iapetus, while Population II seemed to only appear on young terrains of Enceladus, Tethys, Dione, and Mimas.

The hypotheses regarding the sources of these populations, however, varied. Shoemaker and Wolfe (1981), Horedt and Neukum (1984), and Chapman and McKinnon (1986) all suggested that the source for Population I was heliocentric comets and the source for Population II was small planetocentric debris. This planetocentric debris was composed of escaped secondaries from large basins and remnants of disrupted satellites. Meanwhile, Smith et al. (1981, 1982), Strom and Woronow (1982), Strom (1987b), Plescia and Boyce (1985), and Kargel and Pozio (1996) argued that the source for Population I was planetocentric and composed of accretional remnants (note Smith et al. (1981) suggested heliocentric comets as a possibility). Plescia and Boyce (1985) further suggested that the collisionally evolved tail of the accretional remnants was the source for Population II. They contended that the debris created by escaped ejecta and disrupted satellites was not enough to create all the Population II craters. Kargel and Pozio (1996) agreed with this, but advocated that these two impactor sources could combine with smaller heliocentric comets to generate Population II craters. Finally, in opposition to all of these hypotheses, Hartmann (1984, 1995) argued that only one population was recorded, and that differences were caused by saturation equilibrium and resurfacing affecting the crater distributions. He proposed this one population would likely be heliocentric asteroids, comets or some combination of both.

Since July 2004, the *Cassini* spacecraft has been improving on the coverage initially obtained by *Voyager* 1 and 2, and thus has allowed further study and understanding of the mid-size saturnian satellites. The *Cassini ISS* camera has imaged the satellites at >70% coverage at a resolution of 1 km/pixel or better (Fig. 1; Table 1). The *Cassini ISS* camera has also been able to obtain a number (~25) of even higher resolution (<100 m/pixel) images of all the satellites except Mimas (Table 2). With images such as these the cratering records can be extended down to diameters of 1–10 km globally and down to hundreds of meters in local regions. This now allows further analysis of the cratering records of Saturn's mid-sized satellites.

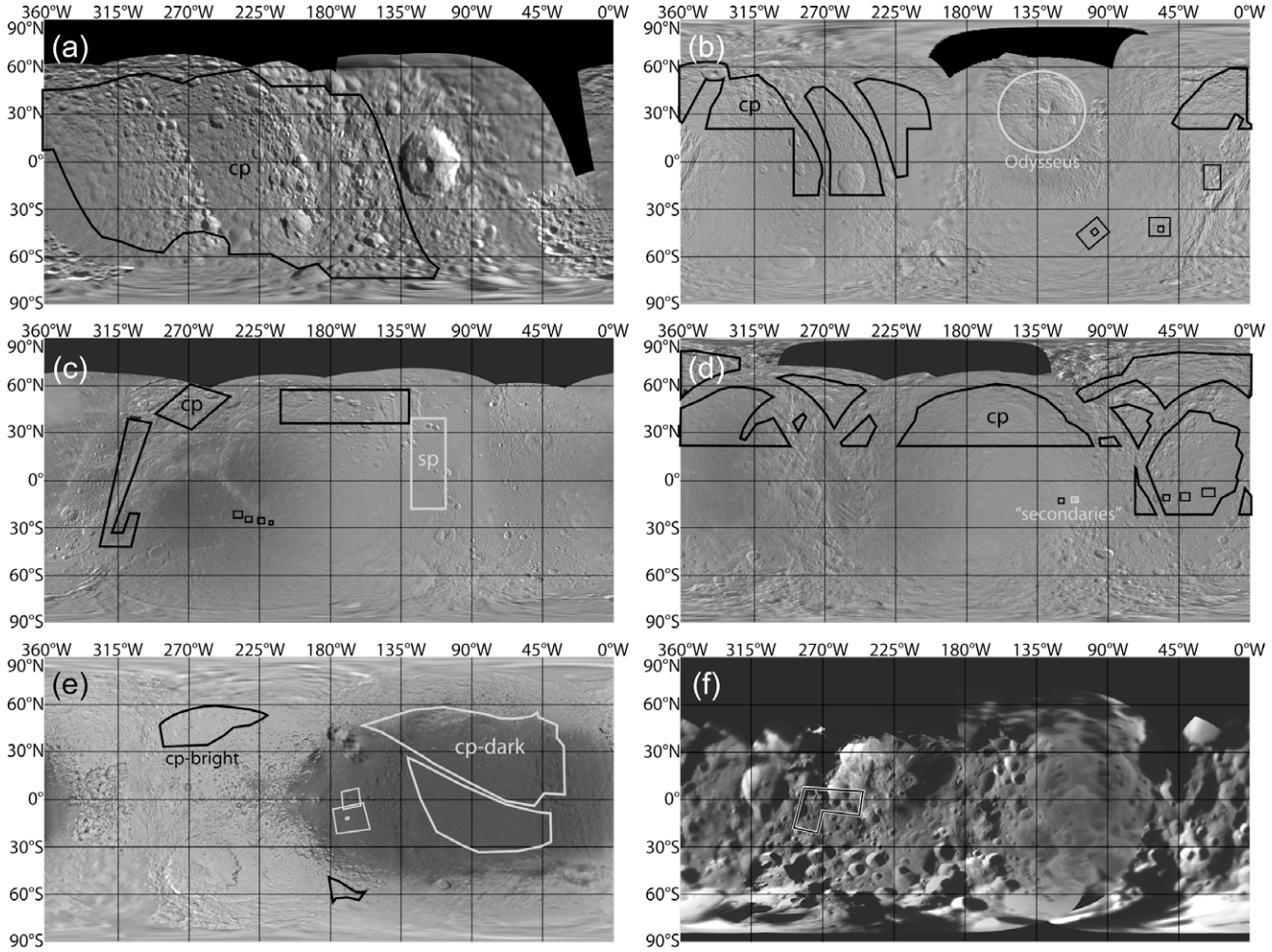

Fig. 1. Global mosaics of: (a) Mimas, (b) Tethys, (c) Dione, (d) Rhea, (e) Iapetus, and (f) Phoebe used to compile the impact crater databases. Mosaic resolutions are given in Table 1. The regions used to compile the crater databases for $D < 100$ km are outlined in each map. The entire mosaic was used to compile craters $D \geqslant 100$ km for Mimas, Tethys, Dione, Rhea, and Iapetus. Smaller boxes indicate positions of high-resolution (*hr*) and very high-resolution (*vhr*) images (details of images given in Table 2). *cp* – cratered plains, *sp* – smooth plains.

Table 1
Global mosaic resolution of Saturn's mid-sized satellites.[a]

Satellite	Resolution (m/pixel)	Satellite	Resolution (m/pixel)
Mimas	400	Rhea	1000
Tethys	400	Iapetus-dark	750
Dione	400	Iapetus-bright	400

[a] Mosaics shown in Fig. 1.

Current work using crater distributions compiled from *Cassini* images has involved preliminary analyses of the geologic histories of Tethys, Dione, Rhea, Iapetus, and Phoebe, and constraining the characteristics of impactor population(s). Analyses of Tethys have been mainly focused on the formation of Ithaca Chasma and its possible relation to the basin Odysseus (Giese et al., 2007), which have indicated that Ithaca's formation is not related to Odysseus' formation. Only one set of work by Neukum et al. (2005) has focused on the computing absolute age of the heavily cratered terrain, but they have exclusively used a lunar chronology. Wagner et al. (2006) have initiated examination of Dione's geology. They have given a description and ages of the heavily cratered, wispy, and smooth plains, but have not determined the full spatial extent of these terrains and their relationships. Wagner et al. (2007) have also begun to explore the global geology of Rhea, but noted there is much work yet to be done. Work on Iapetus has primarily focused on understanding the albedo dichotomy or the equatorial ridge (Neukum et al., 2005; Porco et al., 2005; Denk et al., 2008; Giese et al., 2008; Schmedemann et al., 2008). Analyses of Phoebe's crater distribution (Porco et al., 2005; Richardson et al., 2006; Thomas, 2007) have shown that this irregular satellite had a history dominated by collisions. Finally, initial analyses of impactor populations using *Cassini* imaging have been in disagreement. Neukum et al. (2005, 2006), Wagner et al. (2006), and Schmedemann et al. (2009) argue for only one heliocentric population that is the same as the one bombarding the Moon. Alternatively, Kirchoff and Schenk (2009b) propose that the crater distributions reveal the signature of two populations, similar to the ones found with *Voyager* data (e.g., Chapman and McKinnon, 1986).

These preliminary results have not yet been able to fully constrain the sources of impactor(s) and the geologic histories of the saturnian satellites. Therefore, we here compile and compare our own impact crater distributions of terrains on Saturn's mid-sized satellites Mimas, Tethys, Dione, Rhea, Iapetus, and Phoebe to continue to place constraints on these satellites' geologic histories and on impactor population(s). We do not include Enceladus here as we have a companion paper that focuses on what the impact crater distribution reveals about Enceladus' geologic history (Kirchoff and Schenk, 2009a). Cumulative, differential and relative (R) size-frequency distributions are used to analyze the data.

Our data indicate that for crater diameters less than 4 km and diameters greater than 80 km the distributions in the cratered plains (*cp*) of Mimas, Tethys, Dione, Rhea, and Iapetus are very similar. For craters with diameters between 4 and 80 km, however, the size-frequency distributions for Rhea and Iapetus have constant R-values, while R-values for Mimas, Tethys, and Dione first increase until $D \sim 10$ km, then decrease. This possibly implies that there is one common background impactor population that has bombarded all the satellites, but that has been modified for $4 < D < 80$ km on some of the satellites. One possible modification that agrees with the higher density of relatively smaller craters and lower density of relatively larger craters on Mimas, Dione, and Tethys compared with Rhea and Iapetus is the addition of Saturn Population II as introduced in *Voyager* analyses (e.g., Chapman and McKinnon, 1986) to the background.

Meanwhile, Phoebe's impact crater distribution at small diameters (<2 km) appears to be different from all of the other regular mid-sized satellites. There seems to be a lack of craters of a very narrow size range around 1 km in diameter. The cause of this "dip" is currently unknown. One speculation is that the impactor population for irregular satellites is different and unique to these satellites. There has been some evidence for a similar distribution on the irregular satellites Hyperion, Telesto, and Epimetheus (Richardson and Thomas, 2007; Thomas, 2007). Therefore, the unique distribution may be caused by interactions between the irregular satellites. Another speculation we suggest are that the dip is due to in some way the capture of Phoebe.

Table 2
High-resolution images used to compile impact crater distributions.

Terrains	Image number[a]	Orbit[b]	Resolution (km/pixel)	Center lat./long.
Tethys	1506220559	15	0.1	9°S, 22°W
	1506222501		0.02	31°S, 24°W
	1506222533		0.2 (WA)	43°S, 54°W
			0.02 (NA)	43°S, 55.4°W
	1506222566		0.2 (WA)	46°S, 98°W
			0.02 (NA)	46°S, 98.5°W
Dione	1481766854	[b]	0.45	0°N, 300°W
	1481766978			
	1481767088			
	1481767211			
	1481767266			
	1507745645	16	0.025	21°S, 237°W
	1507745663			25°S, 225°W
	1507745681		0.018	26°S, 225°W
	1507745709			27°S, 215°W
Rhea	1511726954	18	0.035	11°S, 110°W
	1511737558		0.01	10°S, 121°W
	1511737577		0.006	11°S, 110°W
	1511737677		0.01	10°S, 52°W
	1511737694		0.1	9°S, 40°W
	1511737711			7°S, 25°W
Iapetus	1568127661	49	0.1	0°, 163°W
	1568128142		0.022	13°S, 167°W
	1568128143		0.22	13°S, 167°W
Phoebe	1465674412	0	0.015	6°S, 250°W
	1465674502			
	1465674604			
	1465674693			
	1465674782			
	1465674830			
	1465674917			
	1465674956			
	1465675034			
	1465675051			
	1465675070			

[a] Cassini ISS image numbers.
[b] Letters and numbers represent *Cassini* orbits.

2. Methods

2.1. Images

Impact crater distributions are generated from publicly released *Cassini ISS* images, in some cases combined with the highest resolution *Voyager* images where gaps in the *Cassini* images exist. For this analysis, we have recorded craters from controlled global mosaics of Mimas, Tethys, Dione, Rhea, and Iapetus. Table 1 indicates the resolutions and Fig. 1 shows the mosaics and outlines of the regions counted. We have also recorded craters from controlled high-resolution (*hr*) to very high-resolution (*vhr*) images of Tethys, Dione, Rhea, Iapetus, and Phoebe. Descriptions of these images are summarized in Table 2. Placement of the high-resolution images in global context is noted by small boxes in Fig. 1. Regions and images are chosen such that the imaging has neither too

large nor too small solar incidence angle, so that images are not too dominated by shadows for the former or that topography is not well defined by shadows for the latter. Terrains used have incidence angles roughly between 60° and 88°.

Using the global mosaics, we have completed counts for craters with $D \geqslant 100$ km ("basins" in Sections 2–8). Counts generated here for $D < 100$ km, however, are from a considerable number, but not all, of the images suitable for crater recognition (see Sections 2–8). For these diameters, our distributions are preliminary, but should be a good representation of our final distributions. Future work will complete these counts from the remaining images (and new images from *Cassini's* extended mission). After our distributions are finalized, we will compare our results to previous *Voyager* and *Cassini* results to determine how well our dataset compares with others. Comparing crater distributions between different crater counters is currently the best way to verify if the counts are an accurate representation of the distribution.

2.2. Crater counting

Kirchoff's crater counting technique has been described in detail in Kirchoff and Schenk (2009a). Global mosaics (Fig. 1) are divided into preliminary geologic units so that counts from different types of terrains are not combined inappropriately. At least ¼ of the crater rim had to be recognizable to be included in the database. We have tried to reduce contamination by secondaries of the small primary crater databases by not using the few high-resolution and very high-resolution images obviously dominated by dense fields of secondary craters in close association with larger primary craters. We do recognize, however, that distant, isolated secondary craters cannot currently be differentiated with any certainty from small primary craters, and that this contamination may be considerable for diameters (D) less than 1 km (Bierhaus et al., 2001, 2005; Chapman et al., 2002; McEwen and Bierhaus, 2006). Therefore, we do not use crater densities for $D < 1$ km to determine relative ages. The issue of contamination of our counts by secondaries will be revisited in Section 6. Features identified as catenae, or impact crater chains, like those on Ganymede and Callisto (McKinnon and Schenk, 1995), were counted such that each identifiable crater within the chain was included as an individual feature. Finally, the diameter measurements included in the database are $\geqslant$10 times the resolution of the image they are derived from to avoid biases in the distribution at smaller diameters near the resolution limit.

We present the results of our crater counts in two formats. The first is plotting the size-frequency distribution in the relative (or R) plot format (Crater Analysis Techniques Working Group, 1979). The R-plot is the ratio of the differential form of our data to a size-frequency distribution with differential slope equal to −3. The error bars are $\pm N^{0.5}$, where N is the number of craters in a given diameter bin.

The second format is the cumulative and differential slopes of the size-frequency distributions. The cumulative size-frequency distribution is given by (e.g., Melosh, 1989)

$$N(\geqslant D) = c_1 D^{b1}, \tag{1}$$

and the differential size-frequency distribution is given by (e.g., Melosh, 1989)

$$dN(\geqslant D)/dD = c_2 D^{b2}, \tag{2}$$

where c_1 and c_2 are constants and $b1$ and $b2$ are the cumulative and differential slopes. We have calculated the cumulative and differential slopes for certain diameter ranges (see Table 3) of the data shown for each satellite in Supplementary Figs. S1 and S2. The slopes were not calculated for some diameter ranges on each satellite either because the diameter range is not covered by more than two differential bins or the included bins did not contain more than two craters, both of which result in unreliable fits. For these diameter ranges comparisons between size-frequency distributions must remain qualitative. Where appropriate, the slopes and their errors are calculated using a standard linear weighted least squares analysis that minimizes χ^2 (Bevington, 1969). We transform the power-law equations for cumulative and differential size-frequency distributions into log–log space to obtain a linear equation (in a generalized form)

$$\log N = \log c + b \log D. \tag{3}$$

Because of this transformation, the weights cannot be simply set equal to the $N^{0.5}$ error on each data point. These errors must be modified through multiplying by $df(N)/dN$, where $f(N) = \log(N)$. Therefore, the weights are equal to $[(\log(e) * N)/N^{0.5}]^2$, where e is the base of the natural logarithm. Throughout the discussion of the data we will refer to slopes that are "shallow" or "steep". By the label "shallow" we will indicate cumulative slopes $\geqslant -2$ and differential slopes $\geqslant -3$. By the label "steep" we will indicate cumulative slopes < -2 and differential slopes that are < -3.

Table 3
Cumulative and differential slopes.

Terrain	Diameter range (km)	Cumulative slope	Differential slope
Mimas	4–10	−1.548 ± 0.004	−2.1 ± 0.1
	10–30	−2.23 ± 0.02	−2.8 ± 0.3
Tethys-*cp*	0.2–10	−1.701 ± 0.002	−2.71 ± 0.02
	10–65	−2.22 ± 0.02	−3.2 ± 0.2
Dione-*cp*	0.25–4	−1.640 ± 0.007	−2.56 ± 0.07
	4–10	−1.166 ± 0.004	−2.02 ± 0.09
	10–30	−2.31 ± 0.02	−3.2 ± 0.2
	30–150	−2.9 ± 0.1	−3.8 ± 0.4
Dione-*sp*	5–10	−2.21 ± 0.02	−2.5 ± 0.2
	10–45	−2.57 ± 0.08	−3.6 ± 0.4
Rhea-*cp*	0.1–80	−1.823 ± 0.002	−2.77 ± 0.02
Rhea-"secondaries"	0.06–1.5	−2.723 ± 0.006	−3.67 ± 0.06
Iapetus-dark	0.2–4	−1.308 ± 0.004	−2.30 ± 0.04
	4–80	−2.666 ± 0.006	−3.38 ± 0.07
Iapetus-bright	4–65	−1.70 ± 0.01	−2.6 ± 0.1
Phoebe	0.15–1	−2.348 ± 0.002	−2.93 ± 0.04
	1–4	−1.0 ± 0.1	−1.6 ± 0.6

Note: see text for calculation of slopes and errors. *cp* – cratered plains, *sp* – smooth plains.

2.3. Computing ages

We estimate relative ages the terrains discussed here from their cumulative crater densities for $D \geqslant 5$ km. Because we would like to compare ages of terrains from different satellites that have different cratering rates, the crater densities must be scaled to a common rate. Therefore, we use intersatellite diameter scaling for simple craters in the gravity regime as presented in Chapman and McKinnon (1986) to scale the crater diameters on Mimas, Tethys, Dione, Rhea, and Phoebe to their size on Iapetus. Chapman and McKinnon (1986) demonstrated that craters with $D \geqslant 5$ km on the saturnian, icy satellites are formed in the gravity regime using computations of the mechanics of impact crater formation. Meanwhile, McKinnon et al. (1991) demonstrated that complex craters on the icy satellites use the same scaling as simple craters because the transient crater diameter appears to be approximately equal to the final crater diameter for complex craters. Therefore, scaled

crater diameters on the satellites are computed with (Chapman and McKinnon, 1986)

$$D_{scaled} = (g_{Iap}/g_{sat})^{-\alpha/3}(u_{Iap}/u_{sat})^{2\alpha/3}D_{original}, \quad (4)$$

where g_{Iap} and g_{sat} are the surface gravities of Iapetus and the other satellite, u_{Iap} and u_{sat} are the impact velocities on Iapetus and the other satellite, and α is an experimentally determined constant based upon the target material. We use the surface gravities and impact velocities given in Zahnle et al. (2003) for each satellite. We set $\alpha = 0.65$, which is determined for soft rock (Holsapple, 1993) and may be most appropriate for ice. Once the scaled crater diameters are calculated, the scaled cumulative density is computed, and the values are compared to determine relative ages.

For now we have chosen not to compute absolute ages. While cratering rates have been estimated for the saturnian satellites for younger ages ($\lesssim$3 Gyr), the errors on these rates is a factor of 4 (Zahnle et al., 2003), which generally produces error on the ages of more than 2 Gyr. Therefore, the absolute ages for younger terrains cannot be estimated with any precision. Furthermore, ages for the oldest terrains (>3 Gyr) cannot be estimated, because the cratering rates are unknown. Cratering rates do not appear to be constant beyond ~3 Gyr (and possibly even before 3 Gyr) as evidenced through studies of the lunar cratering record (e.g., Bottke et al., 2008), and the dynamical evolution of the outer Solar System impact source regions (e.g., Levison et al., 2008). Therefore, we cannot assume that the current cratering rates calculated by Zahnle et al. (2003) can be extrapolated past ~3 Gyr for the saturnian satellites. Furthermore, current data is insufficient to constrain how cratering rates evolved beyond ~3 Gyr. Did the saturnian system also experience a late heavy bombardment spike like our Moon, or was did the bombardment decline steadily? Finally, although a reasonable cratering chronology has been determined for the Moon (e.g., Stöffler et al., 2006 and references therein), we argue that it cannot be used to date surfaces ages for the outer Solar System because the Moon was likely cratered by a different set of impactors than the Saturn system (e.g., Shoemaker and Wolfe, 1982; Chapman and McKinnon, 1986; Zahnle et al., 1998, 2003).

3. Mimas

Crater counts have been performed for about half of Mimas' surface (Fig. 1). This encompasses almost all of the area that has a suitable resolution and solar incidence angle to adequately recognize craters. While the regions covered by lower resolution (>400 m/pixel resolution of the mosaic) could be counted, the data gained would not be as comprehensive; therefore, we have forgone compiling counts from these regions for now in order to continue to compile more comprehensive crater counts on other surfaces. Data from these regions will be gathered as part of future work.

When combining the data as shown in Fig. 2 with the cumulative and differential slopes given in Table 3 (derived from Supplementary Figs. S1 and S2), we find that Mimas' distribution changes slope. For smaller craters ($D \lesssim 10$ km) the slopes are shallow and R-values slowly increase. The distribution then gets steeper as the craters get larger and R-values decrease. This suggests that the impactor population may be deficient in larger objects. From *Voyager* data, a second population of impactors deficient in larger objects, often referred to as "Saturn Population II", was interpreted to dominate Mimas' cratering record (e.g., Chapman and McKinnon, 1986). This source of the population was debated, but likely seems to be primarily composed of planetocentric impactors. Whatever the source, *Cassini* data also seems to indicate an impactor population deficient in large impactors, at least on Mimas. We explore the possibility of two different impactor populations and their possible sources in Section 9.

4. Tethys

The results presented here will focus on two terrains on Tethys: the heavily cratered terrain and the interior of the large basin Odysseus. Studying the crater distribution of the heavily cratered terrain provides information on Tethys' ancient bombardment history. The distribution within Odysseus provides information about relatively more recent bombardment history, as Odysseus is likely a relatively young basin. The relative age given for the cratered plains and Odysseus in Table 4 indicates that Odysseus could be ~4–9 times younger than the cratered plains. If we assume that the cratered plains are $\gtrsim$ 4 Gyr, then Odysseus could range in age from about 400 Myr to 1 Gyr.

For the heavily cratered terrain we have compiled data from high-resolution images and the global mosaic. *Cassini* has, so far, provided two very high-resolution images of Tethys' heavily cratered terrain with resolutions of 20 m/pixel, along with three high-resolution images with resolutions of 200 m/pixel, that were suitable for crater counting. The global mosaic is at a resolution of 400 m/pixel (Table 1) and most of Tethys' surface is imaged at this resolution (Fig. 1). About 75% of the mosaic also has a solar incidence angle that is good for recognizing craters. We have counted craters on about 1/3 of this available area. This likely provides a reasonable approximation of the distribution of Tethys' heavily cratered plains. Future work, however, will complete these counts to gain our most thorough representation of the distribution and look for spatial density variations across the surface. The data for the interior of Odysseus has been compiled from the global mosaic as well.

Fig. 3 shows the impact crater distributions in R-plot format for Tethys' heavily cratered plains and the interior of Odysseus. We observe from Fig. 3 and Table 3 that Tethys' cratered plains distribution has several changes in slope with increasing diameter. At small diameters the slope is shallow and R-values slowly increase (slope value for $0.2 \leqslant D \leqslant 10$ km), then the slope steepens and R-values decrease for diameters between 10 and 60 km. For $60 < D < 100$ km, the data is insufficient to calculate reliable slope values, but qualitative analysis of Figs. 3, S1, and S2 indicate that R-values decrease more steeply and may imply that the slopes become even steeper. This pattern suggests that the distribution is lacking larger craters with $D \sim 100$ km. On the other hand, the data for Tethys does seem to indicate that more basins with $D > 200$ km are present (i.e., increasing R-values) than would be predicted if the trend for craters between 60 and 200 km continued to larger diameters. This trend also seems to occur on Dione, Rhea, and Iape-

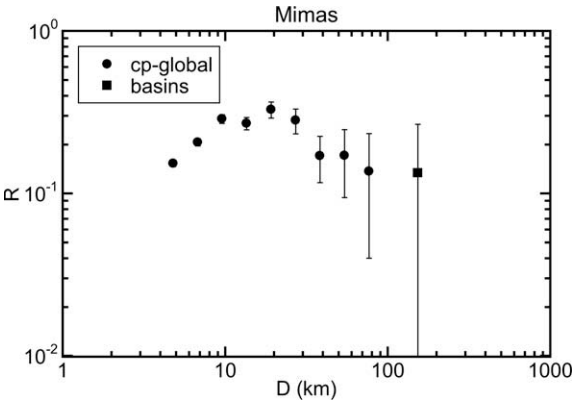

Fig. 2. Relative (R) size-frequency distribution of Mimas cratered plains. The relative plot (R-plot) shows the ratio of the actual distribution to a distribution with a differential slope of −3 in log–log format with $N^{0.5}$ error bars, where N is the number of craters in that bin. Diameters are binned by $(2^{0.5})D$. Mimas' distribution appears to be complex with several slope changes. *cp* – cratered plains, *basins* – craters with $D \geqslant 100$ km.

Table 4
Relative terrain ages for $D \geqslant 5$ km.

Terrain	Cumulative crater density	Scaled density[a]	Relative age to Odysseus[b]	Relative age to Dione-*sp*[b]	Relative age to Mimas[b]
Mimas	4497 ± 136	844 ± 59	4.2–7.3	1.0–1.3	–
Tethys-*cp*	2978 ± 272	910 ± 188	3.8–8.9	⩽1.6	⩽1.4
Tethys–Odysseus	717 ± 71	156 ± 33	–	–	–
Dione-*cp*	2723 ± 1467	1089 ± 823	1.4–15.5	⩽2.8	⩽2.4
Dione-*sp*	2327 ± 112	743 ± 63	3.6–6.6	–	–
Rhea-*cp*	2759 ± 480	1422 ± 531	4.7–15.9	1.1–2.9	1.0–2.5
Iapetus-dark	2687 ± 1501	2687 ± 1501	6.3–34.0	1.5–6.2	1.3–5.3
Iapetus-bright	1846 ± 112	1846 ± 112	9.2–15.9	2.2–2.9	1.9–2.5
Phoebe	2233 ± 1117	1117 ± 790	1.7–15.5	⩽2.8	⩽2.4

Note: *cp* – cratered plains, *sp* – smooth plains.
[a] Cumulative crater density for $D \geqslant 5$ km scaled to Iapetus (see text for description).
[b] Values are the ratio of the scaled density of the terrain specified in the row to the terrain specified in the column header.

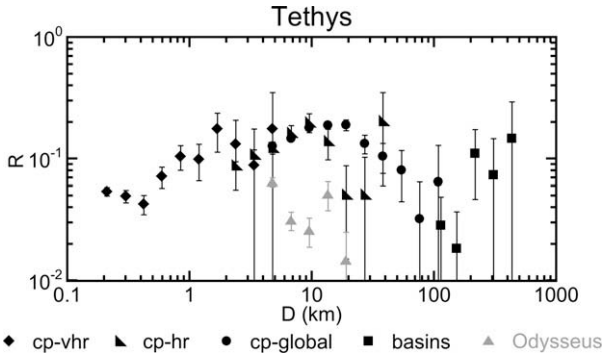

Fig. 3. Relative (R) size-frequency distribution of terrains on Tethys. *hr* – high-resolution, *vhr* – very high-resolution. Other details as described in Fig. 2. The distribution for Odysseus' interior appears different from the distribution for Tethys' cratered plains. This possibly implies the impactor population changed over time at Tethys, as Odysseus is a relatively young basin (Table 4).

tus. The implications of this trend will be discussed further in Section 9, when we compare the distributions.

Finally, we qualitatively compare (Fig. 3) the cratered plains distribution to the distribution for the interior of Odysseus, which is representative of younger terrains. The distributions for the diameter range encompassed ($4 \leqslant D \leqslant 20$ km) appear to be different. While the R-values are increasing for $4 \leqslant D \leqslant 8$ km for the cratered plains, they are decreasing for Odysseus. Then for $D > 8$ km, the R-values have more variation for Odysseus than for the cratered plains. These differences, if real, may indicate that the impactor population changed over time to either gain more small impactors and/or less larger ones, at least for Tethys and crater diameters $4 \leqslant D \leqslant 20$ km. A speculation for the relative increase in small craters on the young terrain is that the flux of Saturn Population II impactors has been more recent. This, however, is not consistent with the hypothesis that Population II is common on Mimas' surface, which is likely older than Odysseus (Table 4). Another speculation is that the flux of Population II impactors has actually been fairly constant through time, and the population is more visible on the younger terrain, which has less overall bombardment to conceal a second population. Additional young terrains need to be imaged at comparable or better resolutions, so that more crater distributions can be compiled and compared, and these possible distribution changes, along with the possible reasons, can be better constrained.

5. Dione

For Dione, our discussion will concentrate on the heavily cratered plains and the smooth plains. Dione's heavily cratered plains likely have not been resurfaced and record ancient bombardment of Dione. The smooth plains, however, are suggested to be an area of resurfacing (Table 4, Smith et al., 1981; Plescia and Boyce, 1982, 1985; Plescia, 1983; Moore, 1984; Morrison et al., 1986; Wagner et al., 2006). The relative ages computed (Table 4) indicate that the smooth plains could be ~3 times younger than the cratered plains. If we assume that Dione's cratered plains are $\gtrsim 4$ Gyr, then the smooth plains may be as young as ~1.5 Gyr. Therefore, studying the crater distribution of the smooth terrains in comparison to the heavily cratered plains may provide information about the temporal evolution of impactors at Dione's orbit.

For Dione's crater plains we have compiled data from four very high-resolution images with resolutions of 25 m/pixel and the global mosaic with a resolution of 400 m/pixel. Approximately 90% of the cratered plains is imaged at ~400 m/pixel, and ~75% of that has the appropriate solar incidence angle for the best crater recognition (Fig. 1). Of the countable area we have recorded craters for ~30% (Fig. 1). This provides a close approximation of the heavily cratered plains distribution. For the smooth plains, we only have the global mosaic to use to compile our database. The smooth plains make up ~30% of Dione's surface (Fig. 1). Most of this has been imaged at 400 m/pixel and has a good viewing geometry for recognizing craters. We have recorded craters for ~50% of this terrain (Fig. 1). Although not complete, these counts supply the necessary data to closely approximate Dione's smooth plains crater distribution. Part of future work will be to complete the global mosaic counts for both the smooth and cratered plains.

For diameters less than 10 km, Dione's cratered plains distribution starts off with a shallow slope and slowly increasing R-values. Then the slope becomes steeper at larger diameters (up to $D = 150$ km), indicating that craters greater than ~50 km are lacking in relation to smaller ones (Fig. 4; Table 3). A relative increase of basins with diameters larger than 200 km is qualitatively indicated in Fig. 4.

When comparing Dione's cratered plains to the plausibly younger smooth plains, the distributions appear similar within error for $10 \lesssim D \lesssim 40$ km, but the distribution on the smooth plains may have a shallower slope for $D < 10$ km (Fig. 4; Table 3). This may imply that the dominant impactor population at Dione gained more relatively large impactors or lost relatively small ones over the possible ~2 Gyr represented. This result is in contrast to the one from Tethys using Odysseus as the representative younger terrain. Conditions could be different from Tethys' orbit to Dione's, especially if the impactor population is dominated by planetocentric debris at Dione (i.e., if the impactor population at Dione was dominated by planetocentric debris early in its history and this population has declined, then a relative decrease in smaller impactors may be expected). Another speculation is that the time frame represented by the smooth plains on Dione and Odysseus is significantly different. Therefore, the two distributions could represent either

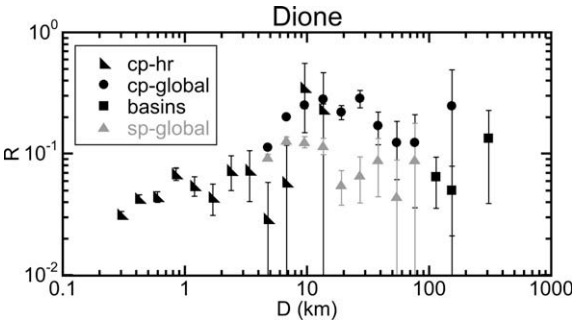

Fig. 4. Relative (R) size-frequency distribution of terrains on Dione. *sp* – smooth plains. Other details as described in Figs. 2 and 3. The lower R-values for the smooth plains imply that they are relatively younger than the cratered plains. The shape of Dione's smooth plains distribution appears to have some similarity to the cratered plains distribution.

the heliocentric or the planetocentric impactor population(s) at different times.

6. Rhea

Presently Rhea does not currently appear to have any large, relatively younger (~same relative age as Odysseus or Dione's smooth plains) terrains imaged at high enough resolution for temporal analysis. Imaging of Rhea, however, has provided high-resolution images of sections of a young, fresh complex impact crater ($D \sim 50$ km) that record a set of potential secondary craters (Fig. 5). We suggest these craters are secondaries based upon their small size ($D < 2$ km), the indication of clustering in some areas, and occasional irregular shapes. The images have resolutions of 6 and 35 m/pixel and provide an excellent opportunity to determine and compare the distributions of secondaries to the cratered plains distribution. This comparison may indicate if crater distributions from heavily cratered regions on Rhea are heavily contaminated by unrecognized secondaries. For this investigation, we only need to recognize that these craters are secondaries and knowledge of the source is not essential. Therefore, we will explore their source, which is currently somewhat ambiguous, as part of a separate investigation that will include the more recent ~45 m/pixel flyby image of this crater.

The counts for the heavily cratered plains are from one very high-resolution image (10 m/pixel), three high-resolution images (100 m/pixel), and the 1 km/pixel global mosaic (Table 2; Fig. 1). Approximately 75% of the global mosaic has sufficient resolution and suitable solar incidence angle to best recognize craters. Of this area, we have counted ~50% (Fig. 1). This provides excellent statistics for much of the diameter range ($1 \leqslant D \leqslant 100$ km) covered and a very good representation of Rhea's cratered plains distribution. Future work will complete these counts to construct a comprehensive global distribution.

Results indicate that Rhea's cratered plains have a relatively simple distribution with only a few slope changes (Fig. 6; Table 3). The slope is generally shallow for the craters range $D = 0.1$–80 km. Then, for $80 \leqslant D \leqslant 200$ km, the rapidly decreasing R-values qualitatively indicate that the slope steepens considerably. This trend implies that smaller basins ($D \sim 100$ km) are more abundant than the larger ones. R-values then increase for $D > 200$ km to indicate that basins

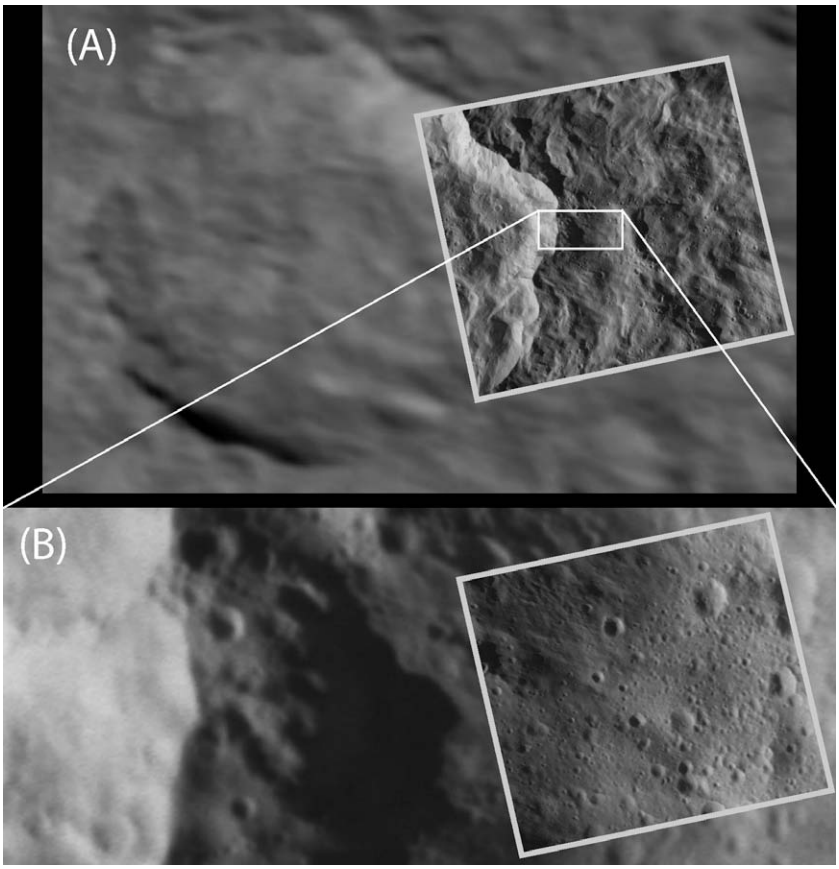

Fig. 5. High to very high-resolution images obtained by *Cassini ISS* of terrain on Rhea near a large primary crater ($D \approx 50$ km) suggested to be dominated by secondary crater fields. (A) High-resolution image (# 1511726954) with a resolution of 35 m/pixel. (B) Very high-resolution image (# 1511737577) with a resolution of 6 m/pixel. Further image details can be found in Table 2.

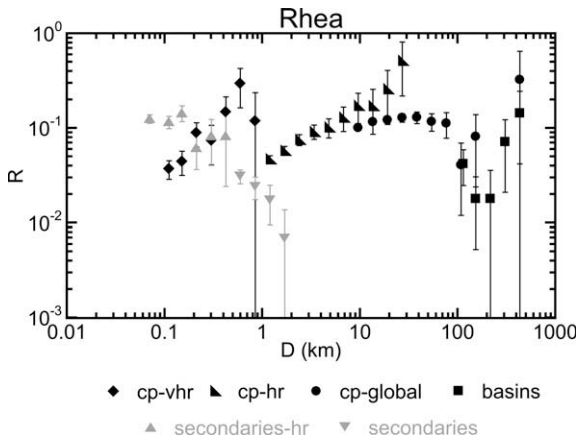

Fig. 6. Relative (*R*) size-frequency distribution of Rhea cratered plains. Details as described in Figs. 2 and 3. Rhea's distribution generally has shallow slopes until $D \approx 80$ km. Basins with $D \sim 150$ km appear to be relatively deficient. The distribution of "secondaries" has a different slope from the cratered plains distribution implying contamination by unidentified secondaries in the cratered plains may be minimal.

~200 km are less abundant than craters larger than 200 km. The distribution for $D < 1$ km, which are the counts from the one very high-resolution image, appears to skew to much higher densities (*R*-values) than might be implied by continuing the trend from the larger diameters. While the data accurately represents the distribution in this *one* very small area (17 km^2), the distribution may not accurately represent Rhea's cratered plains in this diameter range. The larger error bars on the bigger diameter bins ($D > 0.4$ km) of Rhea's distribution from this very high-resolution image imply that the statistics are not very robust and are a result of small number statistics. To resolve this issue and obtain a more accurate representation of the distribution, additional images of Rhea's cratered terrain at comparable resolutions are needed.

When our cratered plains distribution for Rhea, which could have some contamination by secondaries (Bierhaus et al., 2001, 2005; Chapman et al., 2002; McEwen and Bierhaus, 2006), is compared to our distribution from the images likely dominated by secondaries (Fig. 5), the size-frequency distributions ($0.1 \leqslant D \leqslant 1.5$ km) are demonstrated to be very different (Fig. 6; Table 3). As discussed above, the cumulative slope of the cratered plains in the diameter range typically applicable for secondary craters ($0.1 \leqslant D \leqslant 1$ km) is very shallow (~1.8). Meanwhile, the cumulative slope of the presumed secondaries is steeper (~2.7). On the *R*-plot, they cross one another further demonstrating they are two different populations. The steeper slope for the distribution proposed to be secondaries (McEwen and Bierhaus, 2006) supports the hypothesis that this could be a population of craters formed by secondary impacts of ejecta from a nearby crater. To further justify this argument, we will examine in detail the morphology and topography of these craters as part of future work, along with looking for secondaries on the other satellites. Finally, we argue that the very shallow slope and lack of any similarity of the distributions on the *R*-plots implies that our crater plains distribution is relatively uncontaminated by secondaries. While we do not claim that Rhea's (or any other satellites) cratered plains distribution is completely free of secondaries, they appear to be a very minor contribution and are not affecting our overall results.

7. Iapetus

Examination of Iapetus' cratering record focuses on the heavily cratered plains. We have compiled crater distributions on both the bright and dark terrains of Iapetus. For the dark terrain, counts have been obtained from one very high-resolution image (22 m/pixel), two high-resolution images (100 and 220 m/pixel) and a global mosaic with a resolution of 750 m/pixel (Table 2; Fig. 1). In the global mosaic, within the dark terrain, ~60% of the imaging is suitable for recognizing a majority of craters. Of this, we have counted craters from 80%. This provides us with a very good representation of the crater distribution of Iapetus' dark terrain. For the bright terrain, counts have been obtained from a global mosaic with a resolution of 400 m/pixel (Fig. 1). Approximately 30% of the bright terrain is imaged at resolutions and solar incidence angles suitable to best recognize craters. The distribution presented here is compiled from counts incorporating about half of the available area.

Results (Fig. 7; Table 3) indicate that the bright terrain has a similar, if slightly shallower, distribution for craters with diameters between 4 and ~70 km to the dark terrain within error bars. A possible difference, however, is that the dark terrain may have a higher density of craters with diameters between 4 and 10 km (i.e., larger *R*-values). One set of high-resolution data indicates similar densities while another indicates higher densities. This may be further indication that small areas of terrain could have differing size-frequency distribution due to the stochastic nature of impact cratering. With two equally valid datasets indicating two different conclusions, we cannot definitively conclude that the dark and bright terrain distributions are different or the same for this diameter range. The argument could be made that because the distributions are so similar for the larger crater diameters, the data indicating higher densities may be the random variation and the other is the more accurate representation.

Iapetus' cratered plains distribution, making the assumption that the bright and dark terrains record the same impactor population, has a shallow slope for crater diameters between 0.2 and 80 km (Fig. 7; Table 3). For craters with $80 \leqslant D \leqslant 100$ km, the *R*-value data indicates that mid-sized basins ($D \sim 100$ km) are relatively depleted when compared to smaller basins. Finally, the *R*-values increase, indicating that basins with $D \geqslant 200$ km are more numerous. Implications will be discussed in Section 9 when Iapetus is compared to the other satellites, as this tendency does not seem to only occur on Iapetus, as described in previous sections.

8. Phoebe

Lastly, we look at the irregular satellite Phoebe. Phoebe is overall very different from the other satellites mentioned here. It is not round, but potato shaped and small (radius = 106 km) (Smith et al., 1982; Thomas et al., 1986; Porco et al., 2005). Phoebe also has a

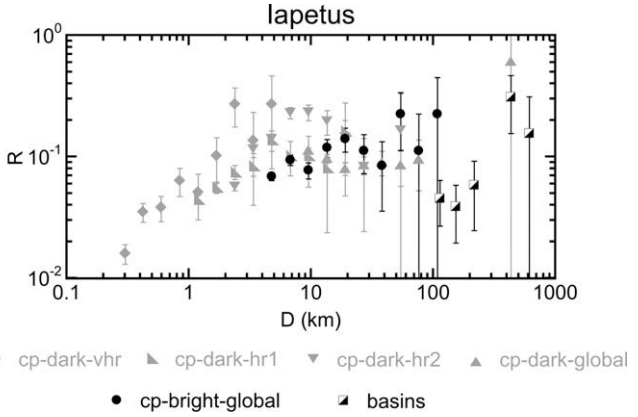

Fig. 7. Relative (*R*) size-frequency distribution of both Iapetus bright and dark cratered plains. Details as described in Figs. 2 and 3. The crater distributions on Iapetus' dark and bright terrains appear very similar within error, where data overlap. This implies that both terrains have had similar geologic histories.

retrograde orbit, is very distant from Saturn, and has a much darker albedo (except for Iapetus' dark terrain) (e.g., Smith et al., 1982; Thomas et al., 1986; Porco et al., 2005). Phoebe's unusual orbit has led some researchers to hypothesize that Phoebe is a captured object (Pollack et al., 1979; Burns, 1986; Cuk and Burns, 2004; Kortenkamp, 2005; Porco et al., 2005; Nesvorný et al., 2007). Phoebe has also likely interacted considerably with the other irregular satellites, such as Hyperion (Nesvorný et al., 2003; Porco et al., 2005). Here we will present the data we have compiled on Phoebe's impact crater distribution from a high-resolution image mosaic (15 m/pixel; Table 2). Presently, we have no counts from the global mosaic, and future work will include compiling a crater database from the global mosaic. Future work will also include determining crater distributions of Hyperion, Epimetheus, Telesto, and Janus for analysis and comparison.

The data from Phoebe indicate that its size-frequency distribution has relatively constant R-values at small diameters ($D \lesssim 1$ km), but then has a sudden and confined dip in R-values around $D \sim 1.5$ km (Fig. 8). Beyond this dip ($D \gtrsim 2$ km) the R-values increase, but error bars get large and the data for these larger diameters may not be as reliable.

The dip is an intriguing feature and difficult to explain. One speculation is that the feature could be related to Phoebe's capture. The feature could have been produced when Phoebe was in another part of the Solar System as part of another population of objects or as Phoebe was being captured (e.g., collisions with another object or flying through a debris field). An argument against this is that a size-frequency distribution similar to Phoebe's has not been found on other bodies outside of the Saturn system. This argument is weakened by the fact that the crater distribution of other small outer Solar System objects has been limited (mainly to the Jupiter system), so we do not have a good database for comparison, which would include Kuiper Belt objects, etc. This distribution, however, has been found on other irregular saturnian satellites, such as Hyperion, Epimethius, and Telesto (Richardson and Thomas, 2007; Thomas, 2007). This might mean that the dip is related to how irregular satellites interact with one another. Numerical modeling of interactions between the irregular satellites would be necessary to determine if this is the case.

9. Intersatellite comparisons of heavily cratered Terrains on Saturn's satellites

Fig. 9 shows the size-frequency distribution (not scaled) for heavily cratered terrains on each satellite for comparison in R-plot format. The presentation of the distributions has been modified (Fig. 9) to simplify the plot and make comparisons more straightforward. The raw data points for each terrain discussed (shown for comparison in Fig. S3 and see Figs. 2–4 and 6–8) have been averaged where data overlaps from different source images and plotted as a connected line without error bars (the line is dashed when it goes through a diameter bin with no data). Where data are averaged the raw R-values are weighted by their errors (similar to the method of Wall and Jenkins (2003, p. 45)), so that values computed using a large number of measurements, which are more reliable, are given more importance in the calculation of the average. This technique is described in more detail in Kirchoff and Schenk (2009a).

Note that data from the dark and bright terrains of Iapetus have also been averaged together where data overlaps. The raw values in Fig. 7 indicate that the two terrains have similar distributions, thus providing reasonable cause to combine the two datasets and allow us to further simplify the R-plot. Of course, we do not have data for $D < 4$ km on the bright terrain. Therefore, we have made the assumption that if the crater size-frequency distribution for these two terrains are similar for larger diameters, then that extrapolates to the smaller diameters. This is not necessarily a well-justified assumption, but no strong evidence is present that the distributions should be different for smaller diameters if they are similar for larger ones. Once we have compiled data for high-resolution images of the bright terrain, we will compare to the dark terrain and determine if this assumption is valid or not.

An initial observation of comparing the satellite's impact crater distributions, is that Mimas and Dione's heavily cratered plains have very similar size-frequency distributions for $D < 80$ km (Fig. 9). Between diameters of 5 and 40 km, the distributions for Mimas and Dione cratered plains practically fall on top of one another. (This qualitative comparison for $4 < D < 30$ km is further supported by the quantitative slope fits in Table 3.) Beyond $D = 40$ km Mimas and Dione's R-values then drop off in a similar manner, until $D \sim 80$ km (Mimas has one crater larger than $D = 80$ km; Fig. S3). The similarity of these two size-frequency distributions implies the same impactor population bombarded Mimas and Dione. The type of impactor population will be discussed shortly, but first the distributions for Rhea and Iapetus will be compared.

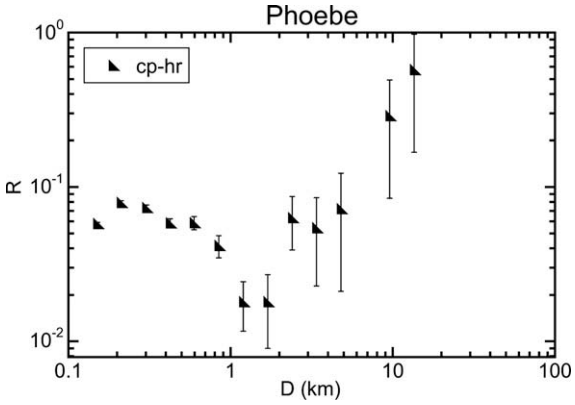

Fig. 8. Relative (R) size-frequency distribution of Phoebe's cratered plains. Details as described in Figs. 2 and 3. Phoebe's distribution is relatively flat on the R-plot for $D < 1$ km, then decreases steeply at $D \sim 1$ km. The distribution then sharply increases at $D \sim 2$ km. This implies that craters with $D \sim 1.5$ km are relatively deficient on Phoebe.

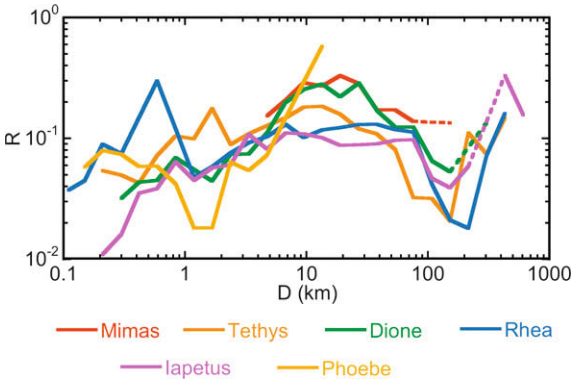

Fig. 9. Relative (R) size-frequency distribution of heavily cratered terrains on Mimas, Tethys, Dione, Rhea, Iapetus, and Phoebe. Raw data from Figs. 3, 4, 6, and 7 that overlap are now averaged as described in the text to facilitate comparisons (all raw data with error bars is plotted in Supplementary Fig. S3 for comparisons). Distributions appear to be very similar for $D < 4$ km and $D > 80$ km on Mimas, Tethys, Dione, Rhea, and Iapetus. For $4 < D < 80$ km, however, Mimas and Dione' distribution are similar, but different from Rhea and Iapetus' distributions, which are similar. Tethys' distribution appears to have characteristics like Mimas, Dione, Rhea, and Iapetus implying Tethys' distribution may be transitional between Mimas and Dione to Rhea and Iapetus. Phoebe's distribution appears to be different from all of these.

The impact crater distributions of Rhea and Iapetus' heavily cratered plains appear to be very comparable. The data shown in Fig. 9 qualitatively demonstrate the correspondence of both the pattern and densities for the two distributions. (The slopes given in Table 3 quantitatively support the similarity for a narrower diameter range.) For the smallest diameters (<1 km), the distributions may diverge in density (Fig. 9), but the data in this range are determined from one small image each for Rhea and Iapetus, and thus the distributions may not be a reliable representation of the actual average distributions for this size range. *R*-values for $10 \leqslant D \leqslant 80$ km are relatively constant, then decrease around $D = 150$ km, only to increase again for the largest basins ($D > 200$ km).

We have noted that the distributions for Mimas and Dione's cratered plains are similar, while the distributions for Rhea and Iapetus' cratered plains are similar. When these two groups are compared (Fig. 9; Table 3), both similarities and differences are observed. For $D < 4$ km, all the heavily cratered plains distributions have slowly increasing *R*-values and shallow cumulative slopes around −1.6. The two groups' distributions begin to diverge at $D \geqslant 4$ km. The *R*-values for Mimas and Dione continue to increase (more steeply than for $D < 4$ km), while Rhea and Iapetus' *R*-values become constant. Then starting at $D = 30$ km, the *R*-values for Mimas and Dione decrease, while *R*-values for Rhea and Iapetus remain constant and do not start decreasing until $D \sim 80$ km. At $D \sim 80$ km, all the satellites' *R*-values begin to decrease sharply, and once again begin to correspond with one another. The distributions reach their lowest density around $D = 150$ km, and then begin to increase for the largest basins (except Mimas, which has no record for these diameters; Fig. S3). Note that for this part of the size-frequency distribution portions of Dione and Iapetus' relative distributions are represented as dashed lines (Fig. 9). As mentioned above, this denotes the fact that no basins with diameters between ~200 and 300 km and 250 and 350 km were actually observed on Dione and Iapetus, respectively. Therefore, the smoothing line, while misleading about the actual crater distribution, may approximate the production function for the impactors, as they are likely to be a continuous distribution. This is also possibly supported by the similarity of the distributions of Tethys and Rhea, which have observable basins of this size, to Dione and Iapetus' distributions. The actual size-frequency distribution of the impactor population, however, is not known, so we cannot conclusively state this is the case. Meanwhile, why are basins of this size not observed on Iapetus and Dione, if the impactors are there? We speculate that they never formed in the first place through random chance.

Tethys' cratered plains size-frequency distribution appears to have characteristics that are transitional between Rhea and Iapetus' distributions and Mimas and Dione's distributions (Fig. 9). For the diameter ranges where the distributions for Mimas, Dione, Rhea, and Iapetus are similar ($\sim 0.1 \leqslant D \leqslant 4$ km and $80 \leqslant D \leqslant 400$ km), Tethys' distribution is also comparable. The *R*-values slowly increase until $D \sim 4$ km and Tethys has a "dip" in *R*-values around $D = 150$ km. For the diameter range between ($4 < D < 80$ km), however, Tethys' size-frequency distribution is not quite like Mimas and Dione's or Rhea and Iapetus'. *R*-values for Tethys appear to slowly increase until $D = 10$ km, then slowly decline until $D = 80$ km, while the *R*-values for Mimas and Dione are more steeply increasing and declining, and the *R*-values for Rhea and Iapetus remain constant. Possibly, Tethys' crater distribution is representing a distribution that is evolving from one pair of satellites to the other.

The variations discussed above in impact crater size-frequency distributions from Mimas and Dione to Tethys to Rhea and Iapetus may be due to either variations in impactor population(s), saturation equilibrium cratering, or alteration of the distributions by geologic processes. First we revisit the possibility of bombardment by two different impactor populations introduced during *Voyager* analyses (see Section 1 and reviewed in Chapman and McKinnon (1986)). Observations from *Voyager* images indicated that heavily cratered terrains, except Mimas, had an impact crater distribution with an abundance of relatively large craters (i.e., flatter on a *R*-plot). Meanwhile, the distribution for young terrains on Dione and Tethys and the heavily cratered terrain of Mimas appeared to be deficient in craters larger than $D \sim 30$ km (i.e., steeply decreasing *R*-values). The leading hypothesis for these differences (see Section 1 and reviewed in Chapman and McKinnon (1986)) was two different impactor populations: Saturn Population I composed of heliocentric ecliptic comets and Saturn Population II composed of planetocentric debris. Our observations from *Cassini* data also indicate that Mimas' crater distribution is relatively deficient in the larger craters ($30 \leqslant D \leqslant 80$ km), i.e., like Saturn Population II, but that the heavily cratered terrains of Tethys and Dione are as well. Only the heavily cratered terrains of Rhea and Iapetus are not deficient in large craters between $D = 30$ and 80 km, similar to Saturn Population I. Unfortunately, the distributions of the couple of younger terrains we have analyzed on Tethys and Dione do not have reliable enough data for $30 \leqslant D \leqslant 80$ km to determine whether these terrains record Saturn Population I or II.

The similarity of our results for Mimas, Rhea, and Iapetus to those from *Voyager* analyses suggests that the hypothesis for two different impactor populations, one heliocentric and one planetocentric, may still be plausible. The heliocentric population is represented by Population I on Rhea and Iapetus and the planetocentric population by Population II on Mimas, Tethys, and Dione. The difference in our results for Dione and Tethys from *Voyager* analyses implies that planetocentric impacts may be more widespread on ancient terrains than previously thought.

Another possible cause for the difference in crater size-frequency distributions from Mimas and Dione to Tethys to Rhea and Iapetus is that the crater distributions have reached saturation equilibrium. Saturation equilibrium is suggested to occur when a surface is so heavily bombarded that the formation of craters is equaled by the obliteration of craters (e.g., Gault, 1970; Hartmann, 1984). Here, we have not explored whether these surfaces are in saturation equilibrium, because interpreting saturation equilibrium from crater distributions is complex and requires numerical modeling of the evolution of the size-frequency distributions. Chapman and McKinnon (1986) demonstrated that different impactor populations result in different saturation equilibrium crater distributions for both shape and density. The crater distribution from a steeper sloped impactor population (cumulative slope <−2) will tend not to retain characteristics of the impactor distribution and converge toward a flat distribution on an *R*-plot (i.e., cumulative slope of −2) (see also Hartmann, 1984; Hartmann and Gaskell, 1997). Meanwhile, the crater distribution from a shallow sloped impactor population (cumulative slope >−2) will approach a quasi-equilibrium distribution and tend to retain characteristics of the impactor distribution. Furthermore, the saturation equilibrium (or quasi-equilibrium) density reached will depend on the dynamic range (i.e., the range of impactor diameters) of the impactor population. The smaller the dynamic range, the higher the density a distribution can reach when approaching saturation. Therefore, the differences in densities between the satellites' distributions and the flat *R*-values of portions of these distributions (Fig. 9) may possibly reflect crater saturation on these different surfaces. The differences may, in fact, be a combination of two different impactor populations with different characteristics (discussed above) in saturation equilibrium on these satellites. Future work will involve collaborations to numerically model the evolution of these impactor populations and crater distributions to determine if saturation equilibrium plays a role in the differences observed in the size-frequency distributions.

Finally, can the differences of our distributions (Fig. 9), however, instead be explained by geologic activity alone altering the distri-

butions? If we assume that the distributions of Rhea and Iapetus, which show little evidence of geologic activity, represent the unaltered distribution, then viscous relaxation could be a candidate to "remove" large craters from the records of Mimas, Dione and Tethys. Burial (for example, by ejecta) would not work because this preferentially removes small craters. Modeling of viscous relaxation has demonstrated that craters with $30 \leqslant D \leqslant 80$ km could be considerably relaxed in a reasonable time frame for a plausibly higher heat flow (Parmentier and Head, 1981; Dombard and McKinnon, 2006; Smith et al., 2007). Viscous relaxation, however, also has a couple of problems. First, while Tethys and Dione have evidence of higher heat flows in the past through resurfacing and remnants of relaxed craters, no strong evidence has been found to support Mimas having a high enough heat flow to considerably relax craters, even early in its history (Ellsworth and Schubert, 1983; Pollack and Consolmagno, 1984; Morrison et al., 1986; Schubert et al., 1986; Multhaup and Spohn, 2007). Second, viscous relaxation of a crater generally leaves remnant topography, as evidenced by palimpsests on Ganymede and Callisto (reviewed in Moore et al. (2004), Pappalardo et al. (2004), and Schenk et al. (2004)), and the many relaxed craters observed on the saturnian satellites (Plescia and Boyce, 1985; Morrison et al., 1986; Kargel and Pozio, 1996; Schenk and Moore, 2007; Smith et al., 2007). Therefore, viscous relaxation is not likely responsible for the difference between the size-frequency distributions of Mimas, Dione, and Tethys vs. Rhea and Iapetus.

Phoebe's distribution, for small (<2 km) crater diameters, is not very similar to any of the other satellites discussed here. The *R*-values decrease as diameters increase up to $D = 1.5$ km, while they are increasing for the other satellites. The confined dip in *R*-values around $D = 1.5$ km is not found at all in the other distributions. Finally, the only vague similarity between Phoebe and the other satellites is the slow increase in *R*-values after $D \approx 2$ km until $D \approx 5$ km, when Phoebe's distribution becomes uncertain. These differences lead us to conjecture that for small craters Phoebe has had a different cratering history from the larger regular satellites. This correlates favorably with the different evolutionary history Phoebe has likely had as well (Pollack et al., 1979; Burns, 1986; Cuk and Burns, 2004; Kortenkamp, 2005; Porco et al., 2005; Nesvorný et al., 2007).

10. Conclusions

The high quality of the *Cassini ISS* imaging provides an excellent opportunity to reexamine the impact crater distributions of the mid-sized saturnian satellites. This imaging has greatly expanded the resolution and spatial coverage beyond that of the *Voyager* imaging. Crater distributions can be determined down to diameters of 4 km for all of the satellites and hundreds of meters for most. Here we have used *Cassini* images to compile and analyze impact crater distributions for terrains on Mimas, Tethys, Dione, Rhea, Iapetus, and Phoebe. Not all available images have yet been utilized, and more are to be obtained in *Cassini's* extended mission; therefore, these are preliminary distributions. The crater distribution of Enceladus' terrains is discussed in a companion paper (Kirchoff and Schenk, 2009a).

Mimas' impact crater size-frequency distribution is found to be complex (Fig. 2; Table 3). Several slope changes are evident. The slope for $4 \leqslant D < 10$ km is generally shallow (>−2, cumulative). For diameters larger than ~10 km the slope steepens slightly, but is still relatively shallow until $D \approx 30$ km. At $D \approx 30$–80 km, *R*-values decrease implying that large craters are less abundant on Mimas.

For Tethys, two terrains are analyzed. A crater distribution has been compiled for the heavily cratered plains and the basin Odysseus. The cratered plains are likely very old, while the interior of Odysseus could be much younger (Table 4). Therefore, by analyzing the two terrains, we may attain information about the bombardment of Tethys through time. Overall, the size-frequency distribution of the cratered plains is complex (Fig. 3; Table 3). For $D \leqslant 10$ km, *R*-values slowly increase with increasing diameter. Then between $D = 10$ km and $D = 60$ km, *R*-values slowly decrease. *R*-values sharply decrease for $D > 60$ km until $D \sim 100$ km, where they start to increase again. This implies that basins with $D \sim 100$ km are less abundant than both slightly smaller craters and larger basins. Meanwhile, the size-frequency distribution within the basin Odysseus is also complex, but generally dissimilar to Tethys' heavily cratered plains (Fig. 3). The *R*-values decrease for increasing crater diameter for $4 < D < 8$ km in Odysseus, while *R*-values increase in the cratered plains. In addition, *R*-values are increasing with diameter for $11 < D < 20$ km within Odysseus while they are decreasing in the cratered plains. These differences between the size-frequency distributions of the two terrains with different relative ages (Table 4) imply that the impactor population at Tethys might have changed over time in this size range.

On Dione we have analyzed two terrains to constrain further the temporal evolution of the impactor population. Crater distributions have been compiled and compared for the heavily cratered and smooth plains. The cratered plains are suggested to be very old, while the smooth plains are likely younger (Table 4). Dione's cratered plains appear to have a very similar distribution to Mimas (Figs. 4 and 9; Table 3). Furthermore, Dione's smooth plains appears to overall have a similar size-frequency distribution to Dione's cratered plains for $\sim 10 < D < 70$ km, but may have a steeper slope for $\sim 5 < D < 10$ km (Fig. 4; Table 3). This implies that the relatively small impactor population for Dione may have decreased over time, but larger impactors have not have changed much over the time frame represented.

The distribution of Rhea's cratered plains appears to be less complex than those found for Mimas, Tethys, and Dione (Figs. 6 and 9; Table 3). The distribution has a shallow slope, with little changes from $0.1 \leqslant D \leqslant 80$ km. *R*-values decrease with increasing diameter from $D \sim 80$ km to $D \sim 200$ km implying the slope becomes steeper. Finally, starting at $D > 200$ km *R*-values increase again.

For Rhea, *Cassini* has also obtained some high to very high-resolution images of a potential set of secondary craters covering part of a fresh, young complex crater ($D \sim 50$ km; Fig. 5). The indication of clustering and small size ($D < 2$ km) of these craters suggests they are secondaries. Meanwhile, the images are comparable in resolution to some images of the cratered plains (Table 2). Therefore, we have compiled a crater distribution that is likely dominated by secondaries to compare to our distributions from regions suggested not to be heavily contaminated by secondaries. Results (Fig. 6; Table 3) indicate that the distribution for the secondaries has a very steep slope, while the general cratered plains has a shallow slope ($0.1 \leqslant D \leqslant 1.5$ km). Therefore, our assumptions about the majority of the cratered plains not likely being heavily contaminated by secondaries may be reasonable.

Impact crater distributions have been compiled for both the dark and light cratered terrains on Iapetus. Results indicate that the two terrains have similar distributions (Fig. 7; Table 3). The distributions have relatively flat *R*-values from $D = 0.2$ to $D \sim 80$ km. Then, from $D \sim 80$ km to $D \sim 200$ km, *R*-values rapidly decrease with increasing diameter. Finally, starting at $D \gtrsim 200$, *R*-values increase again. The similarity of the shape and density of the size-frequency distributions for the dark and light terrains imply they formed at the same time (Table 4).

Finally, we have analyzed the impact crater distribution of the irregular satellite Phoebe (Fig. 8; Table 3). Phoebe's distribution has a steep slope between $D = 0.1$ and 1 km, but then has a shallow

slope for D = 1–4 km. This implies that Phoebe has a deficiency of craters with $D \sim 1.5$ km, which is not found on any of the other satellites (Fig. 9). The reason for this deficiency is currently elusive. A couple of possibilities are: (1) this is characteristic of the impactor population at Phoebe's original location from before Phoebe was captured into the Saturn system, if Phoebe was captured; or (2) this distribution results from collisions and interactions with other irregular satellites. The data are currently insufficient to determine which is the most likely explanation.

When all the distributions are compared, except Phoebe, results indicate that overall the impact crater distributions within the older, heavily cratered plains on each satellite are similar to one another for $D < 4$ km (Fig. 9; Table 3). The distributions also have similar R-values for $D > 80$ km, with the changes indicating a deficiency in basins with diameters around 150 km. The exception is Mimas, which does not have the imaging to obtain crater data for $D < 4$ km and is just too small of a satellite to record the same basin population as the other, larger satellites. This deficiency at $D \sim 150$ km, if a real characteristic of the impactor population, is an interesting feature that may have implications about the evolution of that population. Detailed numerical modeling would be needed to understand these implications and will be addressed in future collaborations. While distributions of these satellites are similar over most of the diameter range examined, differences are found between $4 \leqslant D \leqslant 80$ km. Primarily, Mimas and Dione have increasing R-values for the small diameters (<30 km) and decreasing R-values for the larger diameters (>30 km), while Rhea and Iapetus have constant R-values (Fig. 9; Table 3). Therefore, the distributions on Mimas and Dione appear to be "missing" large craters ($D \sim 80$ km) and have a higher density of craters $\sim 10 < D < 30$ km relative to Rhea and Iapetus. This difference is similar to the one found in *Voyager* analyses (Shoemaker and Wolfe, 1981; Smith et al., 1981, 1982; Strom and Woronow, 1982; Horedt and Neukum, 1984; Plescia and Boyce, 1985; Chapman and McKinnon, 1986; Strom, 1987a; Kargel and Pozio, 1996) and is consistent with the hypothesis that it is due to two different sources of impactors (e.g., Chapman and McKinnon, 1986). One population has a shallow slope (Saturn Population I from *Voyager* literature), is best expressed on Rhea and Iapetus, and is likely heliocentric. (This population may also be recorded for $D < 4$ km and $D > 80$ km on all the satellites as indicated by the similarities in the distributions mentioned above.) The second population has a steeper slope (Saturn Population II from *Voyager* literature), has a relative deficiency of larger craters and more small craters, is primarily expressed on terrains on Mimas, Tethys, and Dione, and is consistent with being planetocentric debris. The source of this debris is most plausibly escaped ejecta from the largest impacts on the saturnian satellites and remains of disrupted small satellites.

Because our distributions are preliminary, we have not yet compared them to previous work both with *Voyager* and *Cassini* data. Future work, once the distributions are finalized, will perform this analysis to determine how well our results compare with others. Comparing different crater counters distributions provides one of the best means of really constraining the impact crater distributions to produce the most accurate representation. After this evaluation, future work will also compare the distributions of these saturnian satellites to the jovian satellites and inner Solar System cratering records. The aim of this comparison, along with dynamical modeling performed by collaborators, is to possibly better constrain the characteristics and number of impactor populations throughout the Solar System.

Acknowledgments

This work has been supported by the NASA Cassini Data Analysis Program and an LPI Postdoctoral Fellow to M. Kirchoff. The authors wish to thank Beau Bierhaus and an anonymous reviewer for their constructive comments, which helped to improve this paper. LPI Contribution #1529.

Appendix A. Supplementary material

Supplementary data associated with this article can be found, in the online version, at doi:10.1016/j.icarus.2009.12.007.

References

Bevington, P.R., 1969. Data Reduction and Error Analysis for the Physical Sciences. McGraw-Hill, New York. 336 pp.
Bierhaus, E.B., Chapman, C.R., Merline, W.J., Brooks, S.M., Asphaug, E., 2001. Pwyll secondaries and other small craters on Europa. Icarus 153, 264–276.
Bierhaus, E.B., Chapman, C.R., Merline, W.J., 2005. Secondary craters on Europa and implications for cratered surfaces. Nature 437, 1125–1127.
Bottke, W.F., Levison, H., Morbidelli, A., 2008. Understanding the impact flux on the Moon over the last 4.6 Gyr. Early Solar System Impact Bombardment. Abstract #3005.
Burns, J.A., 1986. The evolution of satellite orbits. In: Burns, J.A., Matthews, M.S. (Eds.), Satellites. Univ. of Arizona Press, Tucson, AZ, pp. 117–157.
Chapman, C.R., 1983. Saturation equilibrium cratering. Am. Astron. Soc., DPS Meeting #15, Bull. Am. Astron. Soc. 15, 854. Abstract #17.11.
Chapman, C.R., McKinnon, W.B., 1986. Cratering of planetary satellites. In: Burns, J.A., Matthews, M.S. (Eds.), Satellites. Univ. of Arizona Press, Tucson, AZ, pp. 492–580.
Chapman, C.R., Bierhaus, E.B., Merline, W.J., 2002. Styles of cratering on Europa. Lunar Planet. Sci. XXXIII. Abstract #2005.
Crater Analysis Techniques Working Group, 1979. Standard techniques for presentation and analysis of crater size-frequency data. Icarus 37, 467–474.
Cuk, M., Burns, J.A., 2004. Gas-drag-assisted capture of Himalia's family. Icarus 167, 369–381.
Denk, T., Neukum, G., Schmedemann, N., Roatsch, T., Wagner, R.J., Giese, B., Perry, J.E., Helfenstein, P., Turtle, E.P., Porco, C.C., 2008. Iapetus imaging during the targeted flyby of the Cassini spacecraft. Lunar Planet. Sci. XXXIX. Abstract #2533.
Dombard, A.J., McKinnon, W.B., 2006. Elastoviscoplastic relaxation of impact crater topography with application to Ganymede and Callisto. J. Geophys. Res. 111, E01001. doi:10.1029/2005JE002445.
Ellsworth, K., Schubert, G., 1983. Saturn's icy satellites: Thermal and structural models. Icarus 54, 490–510.
Gault, D.E., 1970. Saturation and equilibrium conditions for impact cratering on the lunar surface. Criteria and implications. Radio Sci. 5, 273–291.
Giese, B., Wagner, R., Neukum, G., Helfenstein, P., Thomas, P.C., 2007. Tethys: Lithospheric thickness and heat flux from flexurally supported topography at Ithaca Chasma. Geophys. Res. Lett. 34, L21203. doi:10.1029/2007GL031467.
Giese, B., Denk, T., Neukum, G., Roatsch, T., Helfenstein, P., Thomas, P.C., Turtle, E.P., McEwen, A., Porco, C.C., 2008. The topography of Iapetus' leading side. Icarus 193, 359–371.
Hartmann, W.K., 1984. Does crater "saturation equilibrium" occur in the Solar System? Icarus 60, 56–74.
Hartmann, W.K., 1995. Planetary cratering 1: The question of multiple impactor populations: Lunar evidence. Meteoritics 30, 451–467.
Hartmann, W.K., Gaskell, R.W., 1997. Planetary cratering 2: Studies of saturation equilibrium. Meteor. Planet. Sci. 32, 109–121.
Holsapple, K.A., 1993. The scaling of impact processes in planetary sciences. Annu. Rev. Earth Planet. Sci. 21, 333–373.
Horedt, G.P., Neukum, G., 1984. Planetocentric versus heliocentric impacts in the jovian and saturnian satellite system. J. Geophys. Res. 89, 10405–10410.
Kargel, J.S., Pozio, S., 1996. The volcanic and tectonic history of Enceladus. Icarus 119, 385–404.
Kirchoff, M.R., Schenk, P., 2009a. Crater modification and geologic activity in Enceladus' heavily cratered plains: Evidence from the impact crater distribution. Icarus 202, 656–668.
Kirchoff, M.R., Schenk, P., 2009b. Impactor populations in the saturnian system: Constraints from the cratering records. Lunar Planet. Sci. XXXX. Abstract #2067.
Kortenkamp, S.J., 2005. An efficient, low-velocity, resonant mechanism for capture of satellites by a protoplanet. Icarus 175, 409–418.
Levison, H.F., Morbidelli, A., Vokrouhlick, D., Bottke, W.F., 2008. On a scattered-disk origin for the 2003 EL_{61} collisional family – An example of the importance of collisions on the dynamics of small bodies. Astron. J. 136, 1079–1088.
Lissauer, J.J., Squyres, S.W., Hartmann, W.K., 1988. Bombardment history of the Saturn system. J. Geophys. Res. 93, 13776–13804.
McEwen, A.S., Bierhaus, E.B., 2006. The importance of secondary cratering to age constraints on planetary surfaces. Annu. Rev. Earth Planet. Sci. 34, 535–567.
McKinnon, W.B., Schenk, P.M., 1995. Estimates of comet fragment masses from impact crater chains on Callisto and Ganymede. Geophys. Res. Lett. 22, 1829–1832.
McKinnon, W.B., Chapman, C.R., Housen, K.R., 1991. Cratering of the uranian satellites. In: Bergstralh, J.T., Miner, E.D., Matthews, M.S. (Eds.), Uranus. Univ. of Arizona Press, Tucson, AZ, pp. 629–692.
Melosh, H.J., 1989. Impact Cratering: A Geologic Process. Oxford Univ. Press, New York, 245 pp.

Moore, J.M., 1984. The tectonic and volcanic history of Dione. Icarus 59, 205–220.
Moore, J.M., and 11 colleagues, 2004. Callisto. In: Bagenal, F., Dowling, T., McKinnon, W. (Eds.), Jupiter: The Planet, Satellites, and Magnetosphere. Cambridge Univ. Press, Cambridge, UK, pp. 397–426.
Morrison, D., Johnson, T., Shoemaker, E., Soderblom, L., Thomas, P., Veverka, J., Smith, B., 1984. Satellites of Saturn: Geological perspective. In: Morrison, D. (Ed.), Saturn. Univ. of Arizona Press, Tucson, pp. 609–639.
Morrison, D., Owen, T., Soderblom, L.A., 1986. The satellites of Saturn. In: Burns, J.A., Matthews, M.S. (Eds.), Satellites. Univ. of Arizona Press, Tucson, AZ, pp. 764–801.
Multhaup, K., Spohn, T., 2007. Stagnant lid convection in the mid-sized icy satellites of Saturn. Icarus 186, 420–435.
Nesvorný, D., Alvarellos, J.L.A., Dones, L., Levison, H.F., 2003. Orbital and collisional evolution of the irregular satellites. Astron. J. 126, 398–429.
Nesvorný, D., Vokrouhlický, D., Morbidelli, A., 2007. Capture of irregular satellites during planetary encounters. Astron. J. 133, 1962–1976.
Neukum, G., Wagner, R., Denk, T., Porco, C.C., and the Cassini ISS Team, 2005. The cratering record of the saturnian satellites Phoebe, Tethys, Dione and Iapetus in comparison: First results from analysis of the Cassini ISS imaging data. Lunar Planet. Sci. XXXVI. Abstract #2034.
Neukum, G., Wagner, R., Wolf, U., Denk, T., 2006. The cratering record and cratering chronologies of the saturnian satellites and the origin of impactors: Results from Cassini ISS data. Eur. Planet. Sci. Conf., 610 (abstract).
Pappalardo, R.T., Collins, G.C., Head III, J.W., Helfenstein, P., McCord, T.B., Moore, J.M., Schenk, P.M., Spencer, J.R., 2004. Geology of Ganymede. In: Bagenal, F., Dowling, T., McKinnon, W. (Eds.), Jupiter: The Planet, Satellites, and Magnetosphere. Cambridge Univ. Press, Cambridge, UK, pp. 363–396.
Parmentier, E.M., Head, J.W., 1981. Viscous relaxation of impact craters on icy planetary surfaces: Determination of viscosity variation with depth. Icarus 47, 100–111.
Plescia, J.B., 1983. The geology of Dione. Icarus 56, 255–277.
Plescia, J.B., Boyce, J.M., 1982. Crater densities and geological histories of Rhea, Dione, Mimas and Tethys. Nature 295, 285–290.
Plescia, J.B., Boyce, J.M., 1985. Impact cratering history of the saturnian satellites. J. Geophys. Res. 90, 2029–2037.
Pollack, J.B., Consolmagno, G., 1984. Origin and evolution of the Saturn system. In: Morrison, D. (Ed.), Saturn. Univ. of Arizona Press, Tucson, pp. 811–866.
Pollack, J.B., Burns, J.A., Tauber, M.E., 1979. Gas drag in primordial circumplanetary envelopes: A mechanism for satellite capture. Icarus 37, 587–611.
Porco, C.C., and 34 colleagues, 2005. Cassini imaging science: Initial results on Phoebe and Iapetus. Science 307, 1237–1242.
Richardson, J.E., Thomas, P.C., 2007. Modeling the cratering records of Hyperion and Phoebe: Indications of a shallow-sloped impactor population. Am. Astron. Soc., DPS Meeting #39, Bull. Am. Astron. Soc. 39, 430 (abstract).
Richardson, J.E., Veverka, J., Thomas, P.C., 2006. Large impact features on Phoebe and Hyperion: Early analysis results. Am. Astron. Soc., DPS Meeting #38, Bull. Am. Astron. Soc. 38. Abstract #69.04.
Schenk, P.M., Moore, J.M., 2007. Impact crater topography and morphology on saturnian mid-sized satellites. Lunar Planet. Sci. XXXVII. Abstract #2305.
Schenk, P.M., Chapman, C.R., Zahnle, K., Moore, J.M., 2004. Ages and interiors: The cratering record of the Galilean satellites. In: Bagenal, F., Dowling, T., McKinnon, W. (Eds.), Jupiter: The Planet, Satellites, and Magnetosphere. Cambridge Univ. Press, Cambridge, UK, pp. 427–456.
Schmedemann, N., Neukum, G., Denk, T., Wagner, R.J., 2008. Stratigraphy and surface ages on Iapetus and other saturnian satellites. Lunar Planet. Sci. XXXIX. Abstract #2070.
Schmedemann, N., Neukum, G., Denk, T., Wagner, R., 2009. Impact crater size-frequency distribution (SFD) on saturnian satellites and comparison with other Solar-System bodies. Lunar Planet. Sci. XL. Abstract #1941.
Schubert, G., Spohn, T., Reynolds, R.T., 1986. Thermal histories, compositions and internal structures of the moons of the Solar System. In: Burns, J.A., Matthews, M.S. (Eds.), Satellites. Univ. of Arizona Press, Tucson, pp. 224–292.
Shoemaker, E.M., Wolfe, R.F., 1981. Evolution of the saturnian satellites: The role of impact. Lunar Planet. Sci. XII (Suppl. A), 1–3 (abstract).
Shoemaker, E.M., Wolfe, R.F., 1982. Cratering time scales for the Galilean satellites. In: Morrison, D. (Ed.), Satellites of Jupiter. Univ. of Arizona Press, Tucson, pp. 277–339.
Smith, D.E., Turtle, E.P., Melosh, H.J., Bray, V.J., 2007. Viscous relaxation of craters on Enceladus. Lunar Planet. Sci. XXXVIII. Abstract #2237.
Smith, B.A., and 26 colleagues, 1981. Encounter with Saturn: Voyager 1 imaging science results. Science 212, 163–191.
Smith, B.A., and 28 colleagues, 1982. A new look at the Saturn system: The Voyager 2 images. Science 215, 504–537.
Squyres, S.W., Croft, S.K., 1986. The tectonics of icy satellites. In: Burns, J.A., Matthews, M.S. (Eds.), Satellites. Univ. of Arizona Press, Tucson, AZ, pp. 293–341.
Squyres, S.W., Lissauer, J.J., Hartmann, W.K., 1987. Bombardment history of the Saturn system. I: Spatial and size-frequency distributions of craters. Am. Astron. Soc., DPS Meeting #19, Bull. Am. Astron. Soc. 19, 822–823 (abstract).
Stöffler, D., Ryder, G., Ivanov, B.A., Artemieva, N.A., Cintala, M.J., Grieve, R.A.F., 2006. Cratering history and lunar chronology. Rev. Mineral. Geochem. 60, 519–596.
Strom, R.G., 1987a. The Solar System cratering record: Voyager 2 results at Uranus and implications for the origin of impacting objects. Lunar Planet. Sci. XVIII, 966–967 (abstract).
Strom, R.G., 1987b. The Solar System cratering record: Voyager 2 results at Uranus and implications for the origin of impacting objects. Icarus 70, 517–535.
Strom, R.G., Woronow, A., 1982. Solar System cratering populations. Lunar Planet. Sci. XIII (Suppl. B), 782–783 (abstract).
Thomas, P.C., 2007. Hyperion and its cousins: Sponges, landslides, layers, and ridges. Eos Trans. AGU 88 (52) (Fall Meet. Suppl.). Abstract #P12B-03.
Thomas, P., Veverka, J., Dermott, S., 1986. Small satellites. In: Burns, J.A., Matthews, M.S. (Eds.), Satellites. Univ. of Arizona Press, Tucson, AZ, pp. 802–835.
Wagner, R., Neukum, G., Giese, B., Roatsch, T., Wolf, U., Denk, T., 2006. Geology, ages and topography of Saturn's satellite Dione observed by the Cassini ISS camera. Lunar Planet. Sci. XXXVII. Abstract #1805.
Wagner, R.J., Neukum, G., Giese, B., Roatsch, T., Wolf, U., 2007. The global geology of Rhea: Preliminary implications from the Cassini ISS data. Lunar Planet. Sci. XXXVIII. Abstract #1958.
Wall, J.V., Jenkins, C.R., 2003. Practical Statistics for Astronomers. Cambridge Univ. Press, Cambridge, UK. 277 pp.
Zahnle, K., Dones, L., Levison, H.F., 1998. Cratering rates on the Galilean satellites. Icarus 136, 202–222.
Zahnle, K., Schenk, P., Levison, H., Dones, L., 2003. Cratering rates in the outer Solar System. Icarus 163, 263–289.